IOP Publishing Journal of Physics: Condensed Matter
J. Phys.: Condens. Matter **32** (2020) 175201 (8pp) https://doi.org/10.1088/1361-648X/ab69a0

Efficient metal overlayer catalysts on the Nb_2C monolayer for CO oxidation from first-principles screening

Chang Xu[1], Xilin Zhang[1] and Zongxian Yang[1,2,3]

[1] School of Physics, Henan Normal University, Xinxiang, Henan 453007, People's Republic of China
[2] National Demonstration Center for Experimental Physics Education, Henan Normal University, Xinxiang, Henan 453007, People's Republic of China

E-mail: yzx@henannu.edu.cn (Z Yang)

Received 14 October 2019, revised 10 December 2019
Accepted for publication 8 January 2020
Published 28 January 2020

Abstract

Based on the first-principles calculation, the configurations of different metal overlayers on the monolayer Nb_2C (MXene) (M_{ML}/Nb_2C) (M = Rh, Ir, Pd, Pt, Ag, Au) were studied aiming to find a kind of complex system with high CO-tolerance and high CO conversion efficiency. Combined with the stability of the composite systems and their adsorption properties on small gas molecules, Ag_{ML}/Nb_2C was screened out and further tested for CO oxidation reaction. By comparing the energy barriers of different reaction pathways, we concluded that CO oxidation reaction could be carried out on Ag_{ML}/Nb_2C var the LH mechanism with a small energy barrier of 0.35 eV. The rate-determining step was the oxidation of CO by the adsorbed oxygen atom. The Ag_{ML}/Nb_2C showed good activity for CO oxidation, which would provide a theoretical basis for designing the electrode material for the proton exchange membrane fuel cells (PEMFCs).

Keywords: Nb_2C, MXene, CO oxidation, PEMFCs, metal overlayer

(Some figures may appear in colour only in the online journal)

1. Introduction

As a clean energy device, the proton exchange membrane fuel cells (PEMFCs) has broad application prospects. The H_2 fuel that fed into the PEMFCs anode is usually obtained from fossil fuels, which would inevitably contain CO contaminant. The existence of CO would poison the electrode material, and therefore deactivate the electrode material and lower the energy conversion efficiency. Therefore, the design of electrode materials with high CO-tolerence is a matter of great concern. This requires the electrode materials to be able to catalyze CO oxidation efficiently.

MXenes, a new family of 2D materials, can display different properties by changing the composition and termination [1, 2]. The rich combination forms and excellent properties make MXenes widely explored in many fields [3, 4]. It is possible to tune the number of valence electrons of MXenes and enhance their electronic functionality [5]. MXenes have high specific surface area, which is prominent for catalytic reactions. For example Ti_2C and Mo_2C have been reported to have good CO oxidation activity [6, 7] and effective photocatalytic water splitting activity [8] after surface modification. Nb_2C has been prepared experimentally [9] and has been reported to have good catalytic properties after adding some terminal modifications. In Handoko *et al*'s report [10], Nb_2CO_2 was speculated to have a good activity in catalytic CO_2 reduction process. In Gao *et al*'s calculation [11], from the volcano feature of the average Gibbs free energy of hydrogen adsorption, it is expected that Nb_2CO_2 has a nice catalytic activity in hydrogen evolution reaction (HER). By Pandey *et al*'s screening [12], Nb_2NO_2 was also predicted to have good catalytic activity for HER. Therefore, we have sufficient reasons to believe that the Nb-based MXenes have certain advantages in catalytic activity. However, the CO oxidation reaction has not been

[3] Author to whom any correspondence should be addressed.

reported on the Nb-based MXenes. Due to the high chemical activity of the bare Nb_2C monolayer, loading terminal atoms or functional groups is needed to regulate the surface activity [6]. We expect to find a combination that can form a stable composite system with the bare Nb_2C and meet the expectations mentioned above.

Noble metal catalysts have excellent catalytic efficiency [13–16] and were used as the electrode catalysts for PEMFCs, but the high price greatly limits their practicability. Therefore, it is imperative to reduce the amount of noble metals used in the electrode catalysts. We chose Rh, Ir, Pd, Pt, Ag, Au overlayers as terminals on the bare Nb_2C monolayer. These transition metals have been widely studied for catalytic reactions [17, 18]. Moreover, it has been experimentally implemented that many metal nanoparticles [19] and carbon nanotube [20] can be loaded on MXenes. Few-layered MoS_2 loading on MXenes were also experimentally prepared [21]. It can be speculated that metal monolayers would be possible to form on MXenes. In this paper, we study the configurations of different metal overlayers (M = Rh, Ir, Pd, Pt, Ag, Au) loaded on the bare Nb_2C monolayer (M_{ML}/Nb_2C). The systems with high stability and high activity for CO oxidation will be screened out. We hope to find a combination with high CO-tolerance and high efficiency to catalyze CO oxidation reaction.

2. Computational details

The spin-unrestricted density functional theory (DFT) calculations were performed using the DMol^3 code embedded in Materials Studio with the DNP (double numerical plus polarization) basis sets and DFT semicore pseudopotentials (DSPPs) [22]. Generalized gradient approximation (GGA) of Perdew–Burke–Ernzerhof (PBE) formalism was used for the exchange correction interaction [23]. The Tkatchenko and Scheffler (TS) correction scheme was used to describe the van der Waals interaction between layers [24]. The convergence criteria were set to be 10^{-5} Ha for the energy, 0.002 Ha Å^{-1} for the forces, and 0.005 Å for the displacements during the structural optimization. The Brillouin zone sampling was performed using the Monkhorst–Pack Method [25] with *k*-points grids of $15 \times 15 \times 15$ and $5 \times 5 \times 5$ for the optimization of the unit cell and supercell, respectively, and $11 \times 11 \times 11$ for electronic properties calculations. A periodic cell of $10 \times 10 \times 10$ Å was used for the simulation of single atoms and free gas molecules. The linear synchronous transit (LST)/quadratic synchronous transit (QST) method [26] was used for transition states and the minimum energy pathway (MEP) search.

The adsorption energy E_{ad} was defined as:

$$E_{ad} = E_{adsorbate/substrate} - E_{adsorbate} - E_{substrate} \quad (1)$$

where $E_{adsorbate/substrate}$, $E_{adsorbate}$ and $E_{substrate}$ are the total energies of the substrate with adsorbate, the free adsorbate and the bare substrate, respectively. A negative E_{ad} value indicates that the adsorption process is exothermic.

The binding energy E_b per metal atom in the metal overlayers on Nb_2C monolayer was calculated following the equation:

$$E_b = 1/n\left(E_{ML/Nb_2C} - E_{Nb_2C} - nE_M\right) \quad (2)$$

where E_{ML/Nb_2C} and E_{Nb_2C} are the energies of the Nb_2C monolayer with and without metal overlayer, respectively. E_M is the energy of a free metal atom, and 'n' is the number of metal atoms in the metal overlayer.

The cohesive energy (E_{coh}) between the metal atoms in the metal bulk is defined as:

$$E_{coh} = 1/n\left(E_{bulk} - nE_M\right) \quad (3)$$

where E_M and E_{bulk} are the energies of a free metal atom and the unit cell of bulk metal, respectively.

3. Results and discussion

The calculated lattice parameter of the Nb_2C monolayer is 3.059 Å, which is in good agreement with the value obtained by Khazaei *et al* [27]. The space group of the Nb_2C monolayer is $P\bar{3}ml$. A supercell with a 3×3 surface of the Nb_2C monolayer was chosen as the substrate to load the different metal overlayer, as shown in figure 1(a). A vacuum layer of 15 Å was added in between the Nb_2C layers to eliminate the interaction between the periodical images.

3.1. The systems loaded with different metal overlayers

After the Nb_2C monolayer is obtained, we study the configurations of different metal overlayers loaded on Nb_2C monolayer. We first need to select the most favourable adsorption site for all kinds of single metal atoms on Nb_2C monolayer. By comparing the adsorption energies of single metal atoms (Rh, Ir, Pd, Pt, Ag, Au) at different adsorption sites on the Nb_2C monolayer, as shown in figure 1(a) and table 1, we found that all the metal atoms tended to be adsorbed at site 1, the face-centered cubic (fcc) sites. Therefore, the model of Nb_2C monolayer loaded with different metal overlayers was build as shown in figure 1(b), represented by Ag_{ML}/Nb_2C. In order to investigate whether these composite structures have good stability, the E_b and E_{coh} were calculated as shown in table 1, from which we concluded that all of the loaded metal atoms had a larger absolute E_b values than their corresponding absolute E_{coh} values. In other words, the adsorption strength of metal atoms on the Nb_2C monolayer is stronger than the cohesion of metal atoms in bulk. Therefore the low coverage of metal atoms would form single layer on the Nb_2C rather than to form metal bulk or clusters.

3.2. The adsorption of small gas molecules

The adsorption strength of gas molecules is very important to the reaction processes. We hope to screen out the systems with the appropriate adsorption energies for gas molecules. The adsorption energies for the most preferred adsorption configurations of O_2, CO and CO_2 on M_{ML}/Nb_2C were calculated and the results were shown in table 2. For Rh and Ir, the adsorption energies of CO are 2.00 eV and 1.93 eV,

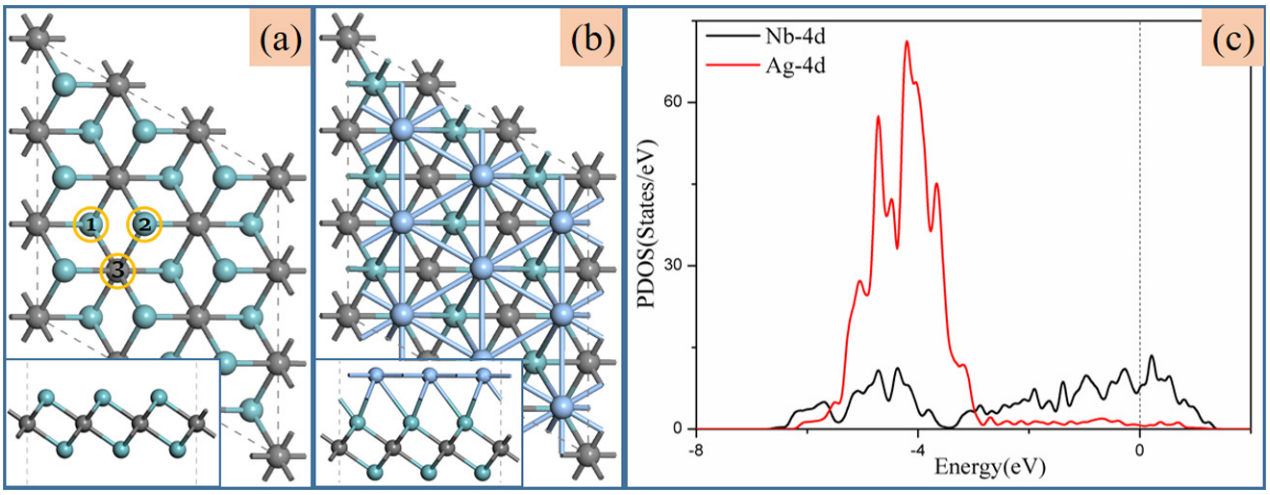

Figure 1. (a) The top and side views of the Nb_2C monolayer, where the gray, and aqua blue spheres represent carbon and niobium atoms, respectively. The numbers 1, 2 and 3 represents different adsorption sites. (b) The top and side views of Ag_{ML}/Nb_2C, where the stone blue spheres represent the adsorbed silver atoms. (c) The partial density of states (PDOS) of Nb-4d and Ag-4d in Ag_{ML}/Nb_2C. The Fermi level is set to be the energy zero (the dotted line represents the Fermi energy).

Table 1. The adsorption energies of different sites for various single metal atoms on bare Nb_2C. The configurations in which the adsorption energy represented by '—' in the table are unstable. When these structures are optimized, they transformed into one of the other two structures mentioned in the figure 1(a).

	E_{b1} (eV)	E_{b2} (eV)	E_{b3} (eV)
Rh	−6.833	—	−6.559
Ir	−8.034	—	−7.725
Pd	−4.865	—	−4.708
Pt	−6.896	—	−6.710
Ag	−3.523	—	−3.498
Au	−4.454	—	−4.416

Table 2. The cohesive energies (E_{coh}) per atom in metal bulk and the binding energy (E_b) per metal atom in the M_{ML}/Nb_2C.

	E_{coh} (eV)	E_b (eV)
Rh	−6.42	−7.26
Ir	−7.56	−8.41
Pd	−3.81	−5.12
Pt	−5.59	−7.03
Ag	−2.99	−3.80
Au	–3.24	–4.51

respectively. Moreover, the adsorption strength of CO is much larger than those of O_2. Therefore CO tends to be adsorbed on the substrate first, which may cause CO-poisoning and deactivate the catalyst. The similar problems existed with the Pd and Pt overlayers. As for Au, the adsorption of O_2 is weak with an adsorption energy of 0.38 eV. Therefore Au_{ML}/Nb_2C may not be sufficiently capable of capturing O_2. It would be possible that the oxygen molecules migrate before reacting with CO. When the adsorption energy of CO is close to that of O_2, it may be easier to form a co-adsorption configuration, which would be beneficial for further reaction. This is the case for the Ag overlayer on Nb_2C, which has adsorption energies of 0.67 and 0.66 eV for O_2 and CO, respectively. To sum up, we finally selected the Ag_{ML}/Nb_2C system as a promising candidate catalyst for CO oxidation reaction. From the partial density of states (PDOS) of Ag_{ML}/Nb_2C shown in figure 1(c), we can see that the Ag-4d states resonate strongly with the Nb-4d states from −8 eV to −3 eV relative to the Fermi level, with their main peaks overlaped to a large extent. This to some extent may also reflect that the Ag_{ML}/Nb_2C has a good stability. The atomic structures and the charge density difference maps for the systems of Ag_{ML}/Nb_2C with small molecules were shown in figure 2.

As shown in figure 2(a), O_2 was adsorbed on Ag_{ML}/Nb_2C in a configuration nearly parallel to the Ag_{ML}/Nb_2C surface with an adsorption energy of 0.67 eV and the O-O bond was stretched to 1.385 Å. In figure 2(b), CO was adsorbed vertically on the substrate, with an adsorption energy of 0.66 eV. We can also see that CO_2 was adsorbed parallel to the substrate in figure 2(c). As seen from the CDD, there was almost no electron transfer between CO_2 and the substrate, reflecting the weak adsorption of CO_2. The adsorption energy shown in table 3 also shows that CO_2 binds to the substrate by physical adsorption. On Ag(1 0 0), the adsorption energy of O_2 (0.11 eV) is much smaller than that of CO (0.35 eV), which is not conducive to the capture of O_2 [28]. Similarly on Ag(1 1 1), the adsorption energy of CO (0.29 eV) is higher than that of O_2 (0.16 eV) [29]. And CO_2 is weakly adsorbed on both of them. CO-poisoning may occur on Ag(1 0 0) and Ag(1 1 1), since CO is more favorable to be adsorbed on the substrate than O_2. The problem on Ag_{ML}/Nb_2C is much less likely to occur, because the adsorption energy of O_2 on Ag_{ML}/Nb_2C is very close to that of CO. Compared with Ag(1 0 0) and Ag(1 1 1), Ag_{ML}/Nb_2C has a higher CO-tolerence.

3.3. The oxidation of CO on Ag_{ML}/Nb_2C

3.3.1. The dissociation of O_2. First, we explored the dissociation process of O_2 on Ag_{ML}/Nb_2C. As shown in figure 3, the barrier for oxygen dissociation reaction is as high as 1.61 eV.

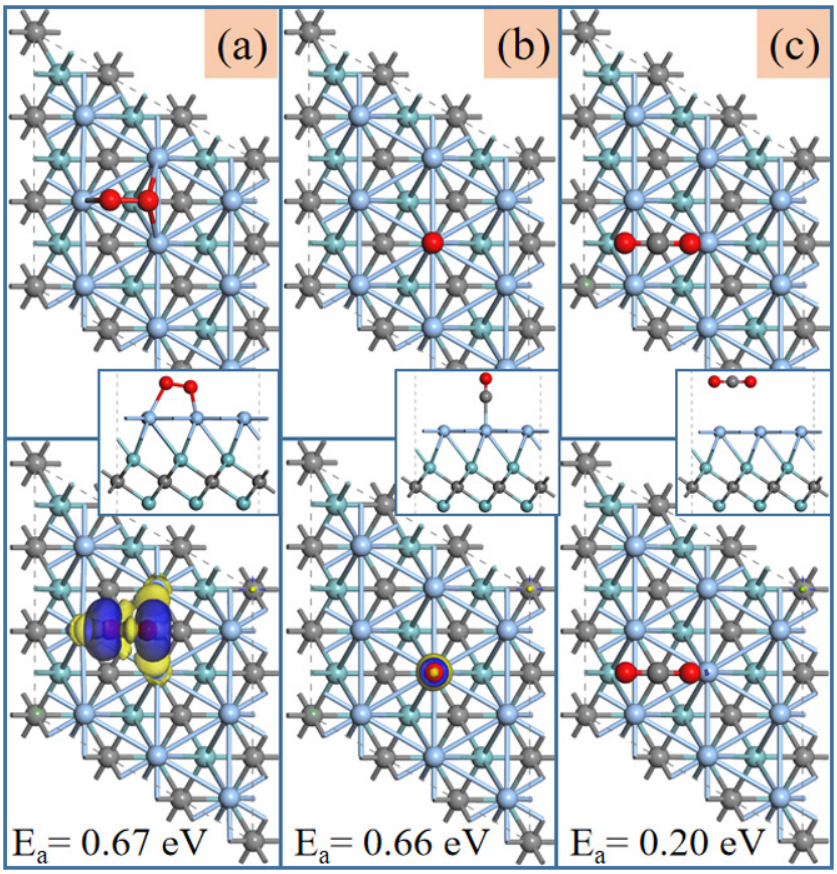

Figure 2. The top and side views of the atomic structures and the charge density difference (CDD) for the systems with O_2 (a), CO (b), CO_2 (c) adsorption on Ag_{ML}/Nb_2C, respectively.

Table 3. The adsorption energies of O_2, CO and CO_2 on M_{ML}/Nb_2C.

	O_2 (eV)	CO (eV)	CO_2 (eV)
Rh	−1.26	−2.00	−0.35
Ir	−1.03	−1.93	−0.26
Pd	−0.73	−1.09	−0.21
Pt	−0.69	−1.35	−0.22
Ag	−0.67	−0.66	−0.20
Au	−0.38	−0.73	−0.20

Therefore, when O_2 is adsorbed on the substrate, the dissociation of O_2 would be difficult. Next, we explored the possible mechanisms of CO oxidation on Ag_{ML}/Nb_2C.

3.3.2. The possible mechanisms of CO oxidation. The CO oxidation reaction may proceed by three mechanisms according to the gas adsorption in the initial structure of the reaction. As shown in figure 4, O_2 was pre-adsorbed on the substrate, and then CO entered to break the O–O bond forming the intermediate CO_3. This is the Eley–Rideal (ER) mechanism [30] for CO oxidation. The process experienced a high barrier of 2 eV for CO breaking the O–O bond. From the perspective of dynamics, the occurrence of CO oxidation on Ag_{ML}/Nb_2C would not be inclined to happen var the ER mechanism. The large oxygen dissociation barrier could explain the phenomenon that a high barrier is required in the process of O–O bond fracture in the ER mechanism.

As shown in figure 5(a), O_2 and CO were co-adsorbed on Ag_{ML}/Nb_2C. The oxidation of CO starting from the co-adsorption structure of O_2 and CO on the substrate was called the Langmuir–Hinshelwood (LH) mechanism [31]. Figure 5(b) showed the intermediate state OOCO in the LH mechanism. We had another co-adsorption configuration as shown in figure 5(c). Unlike the configuration shown in figure 5(a), where the CO was adsorbed above the straight line of the two adsorbed oxygen atoms, the position of CO in figure 5(c) formed a triangle with the two adsorbed oxygen atoms. The adsorption energies of the two co-adsorption configurations are very close (1.40 eV and 1.41 eV, respectively), which are all larger than the sum of the individual adsorption energies of O_2 and CO, indicating that there was mutual attraction between the co-adsorbed O_2 and CO. Moreover, the distance between O_2 and CO is moderate, which is suitable for the further reaction process. LH (l) and LH (t) were used to represent the reaction pathways starting of the co-adsorption configurations in a straight line and the triangle configurations in the following discussion, respectively.

The reaction passways of the LH mechanism starting from the two different initial adsorption configurations were shown in figures 6(a) and (b), respectively. From LH (l) shown in figure 6(a), the formation of OOCO had an energy barrier of

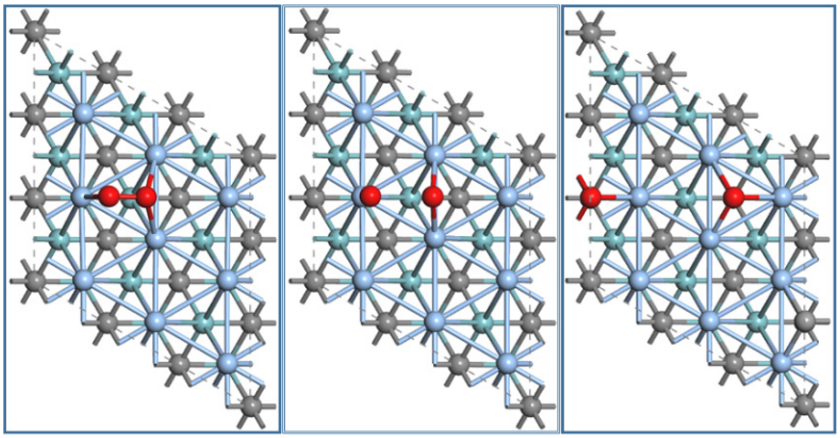

Figure 3. The dissociation process of the adsorbed O_2 on Ag_{ML}/Nb_2C.

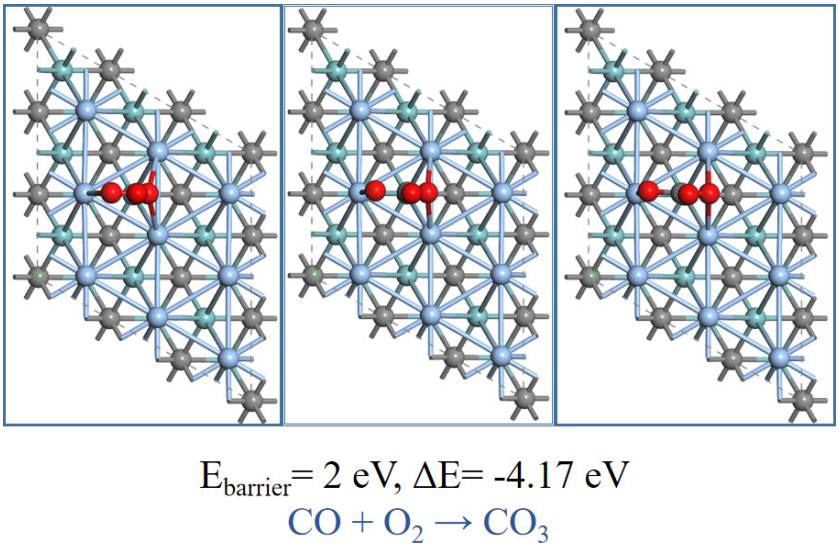

Figure 4. The formation of CO_3 in the Eley–Rideal (ER) mechanism on Ag_{ML}/Nb_2C.

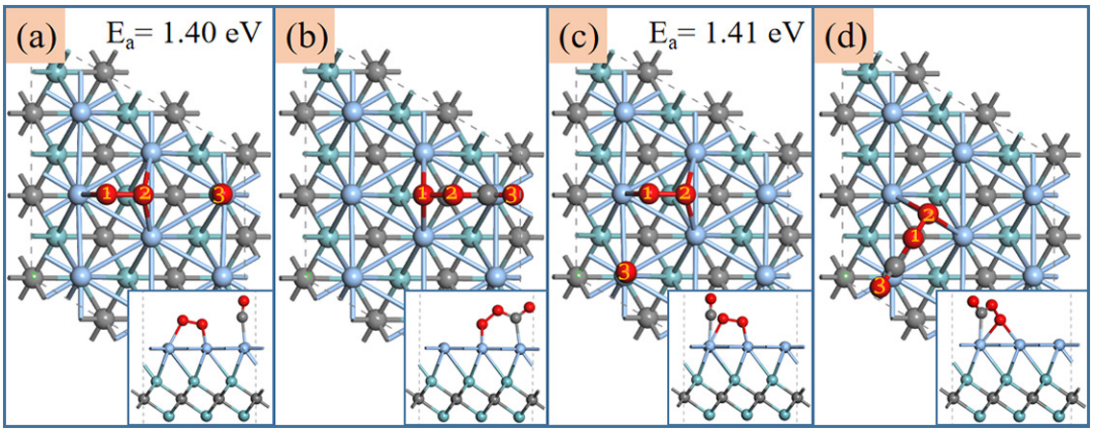

Figure 5. Different initial adsorption configurations (a) and (c) and corresponding intermediates (b) and (d) OOCO in the LH mechanism mechanisms on Ag_{ML}/Nb_2C. The yellow numbers on the sphere label the oxygen atoms.

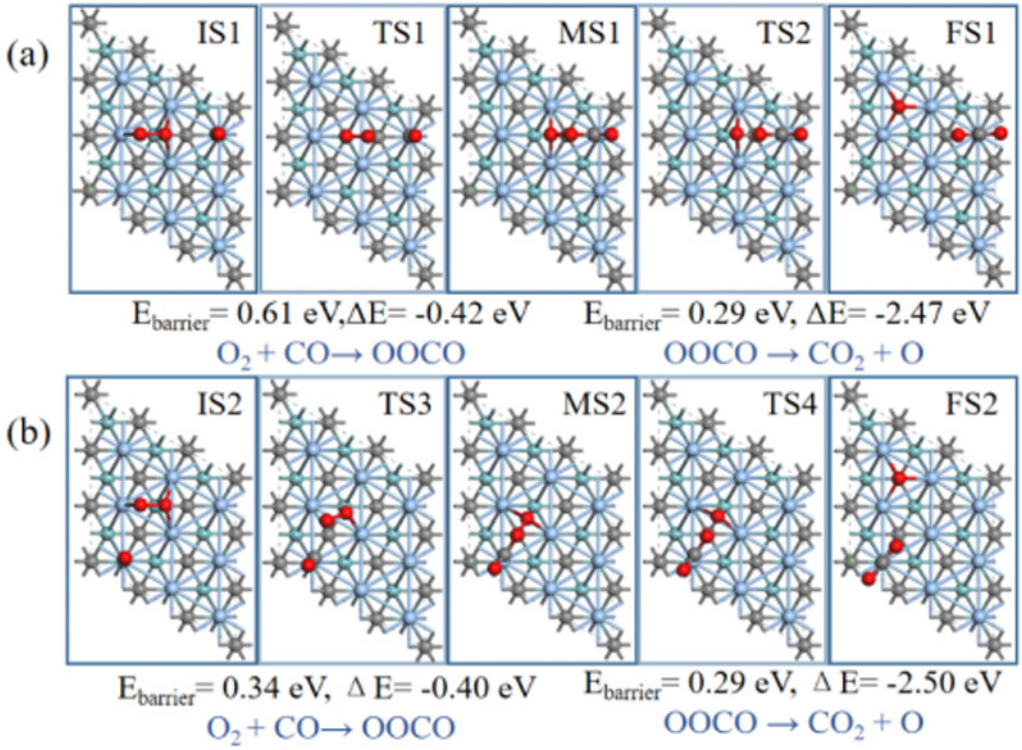

Figure 6. Partial reaction pathway of the LH mechanism from two different initial structures, LH (l) (a) and LH (t) (b) on Ag_{ML}/Nb_2C.

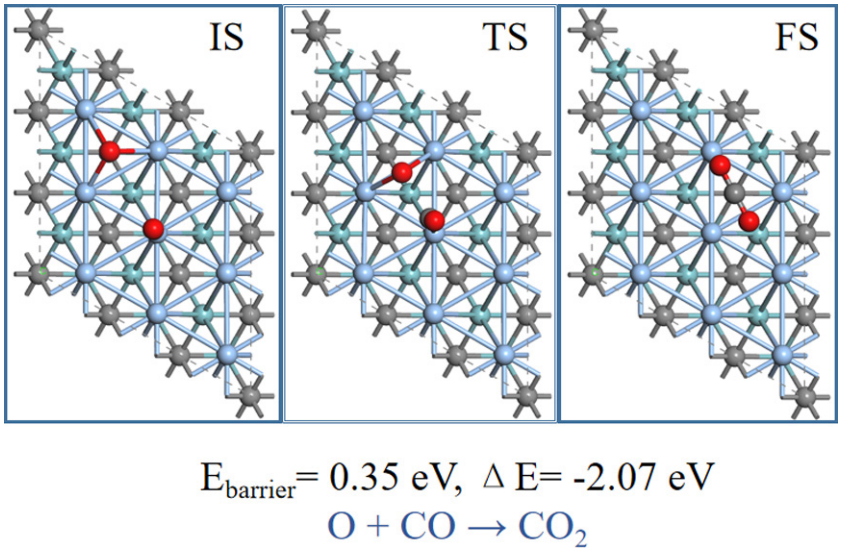

Figure 7. The oxidation of CO by the adsorbed oxygen atom in the LH mechanism on Ag_{ML}/Nb_2C.

0.61 eV, and then the OOCO dissociated further to form an adsorbed oxygen atom and a CO_2 with an energy barrier of 0.29 eV. The most stable adsorption site of the dissociative oxygen atom was at the top of carbon atom, with an adsorption energy of 0.72 eV, while the formed CO_2 was bound to the substrate in the form of physical adsorption. In contrast, the formation of OOCO in LH (t) shown in figure 6(b) had a smaller energy barrier of 0.34 eV. The OOCO in LH (t) is equivalent to that in LH (l) considering the symmetry of the Ag_{ML}/Nb_2C. After the CO_2 was desorbed, both the LH(l) and LH(t) passways ended up with the same adsorbed oxygen atom. The remaining oxygen atom on Ag_{ML}/Nb_2C overlayer may co-adsorb with another CO with a co-adsorption energy of 1.46 eV, which is also larger than the sum of the adsorption energies of an oxygen atom and CO, indicating that the remaining oxygen atom would promote the adsorption of another CO. The oxidation of CO by the adsorbed oxygen atom would need to overcome a barrier of 0.35 eV to form a new CO_2, as shown in figure 7. All the steps in the reaction passway were exothermic.

In order to further explore the reason for the difference in the reaction barriers between the two different reaction pathways

Table 4. Muliken charges of two initial co-adsorption configurations in LH (l) and LH (t) and the corresponding intermediate states OOCO. The atomic labels were shown in figure 5. A negative value indicates that the atom gained electrons and was negatively charged, while a positive value indicates that the atom lost electrons and was positively charged. The values are in $|e|$.

	O1	O2	C	O3
l-CO + O_2	−0.310	−0.349	0.079	−0.069
t-CO + O_2	−0.340	−0.315	0.079	−0.069
l-OOCO	−0.449	−0.153	−0.204	−0.319
t-OOCO	−0.154	−0.450	−0.203	−0.318

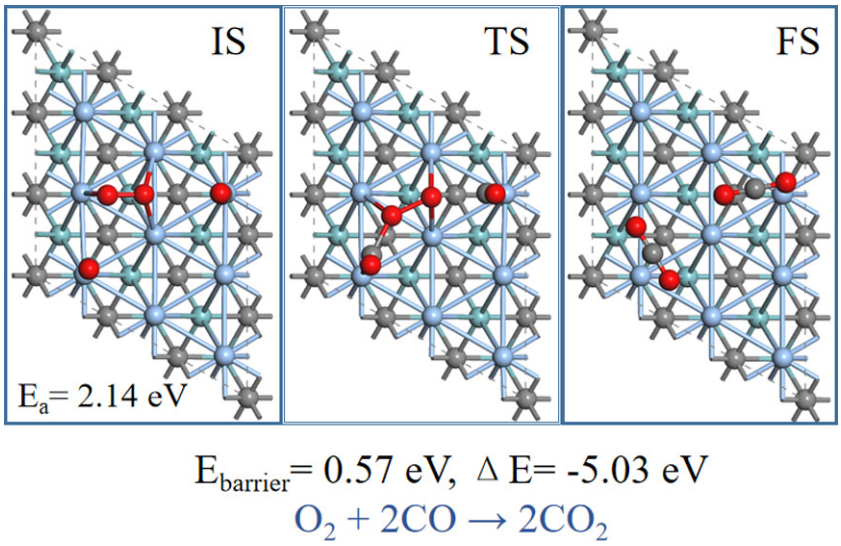

Figure 8. Reaction pathway of CO oxidation reaction through termolecular Eley–Rideal (TER) mechanism on Ag_{ML}/Nb_2C.

in the LH mechanism, we also calculated the Muliken charges of the two initial co-adsorption configurations and the corresponding intermediate states OOCO, as shown in table 4.

From table 4, we can see that, for different initial adsorption configurations, there were different charges on the oxygen atoms, due to the rearrangement of the electrons caused by the proximity of the carbon atom to the different oxygen atom and the unequal distance between the carbon atoms and the nearest oxygen atoms. In both cases, the gain and loss of electrons were basically the same for the corresponding atom of OCOO. In LH (l), the oxygen atom labeled number 2, which has a higher absolute value of charge (0.349), approaching the adsorbed CO, had to overcome the force of two silver atoms closer to it and the oxygen labeled number 1. But in LH (t), the oxygen atom labeled number 1, which has a lower absolute value of charge (0.315), approaching the adsorbed CO, just had to overcome the force of one silver atom close to it and the oxygen atom labeled number 2. Maybe this is the reason why the energy barrier of forming OOCO in LH (t) is smaller than that in LH (l).

The termolecular Eley–Rideal (TER) [32] mechanism would occur when one O_2 co-adsorbed with two CO as shown in figure 8, which had a co-adsorption energy of 2.14 eV on Ag_{ML}/Nb_2C. Just like the co-adsorption of one CO and one O_2, the co-adsorption energy of the three molecules was greater than the sum of their individual adsorption energies, indicating that the formation of the co-adsorption configuration was favorable on Ag_{ML}/Nb_2C. In the TER mechanism, each CO pulled on the oxygen atoms of the co-adsorbed O_2 to form two CO_2 after overcoming an energy barrier of 0.57 eV. The process had a large energy gain of 5.03 eV.

From the respective of the reaction barrier, the oxidation of CO on Ag_{ML}/Nb_2C tends to be carried out var the LH(t) passway, with a barrier of 0.35 eV. To show that Ag_{ML}/Nb_2C is superior for CO oxidation reaction, we compared the CO oxidation reaction barriers of the corresponding rate-determining steps of other systems as shown in table 5. In Zhang's *et al*'s report, the CO reaction process was investigated on Pd(1 0 0) and Pd(1 1 1). Athough the two systems have the same rate-determining step as that on Ag_{ML}/Nb_2C, i.e. the oxidation of CO by the adsorbed oxygen atom, the barrier in Ag_{ML}/Nb_2C (0.35 eV) is significantly lower. In Su *et al*'s report, it had to overcome an even higher barrier (1.03 eV) on Ag(1 1 1) to complete the reaction. In Zhao *et al*'s report, $Ag_{ML}/WC(0\,0\,0\,1)$ was studied. Compared with Ag_{ML}/Nb_2C, both of them were loaded with the same metal monolayer and had the same rate-determining step, however, the combination of Ag overlayer and Nb_2C is more favorable in catalyzing CO oxidation. In Xu *et al*'s report, the catalytic CO oxidation reaction on the Mn-doped graphene ststem reached the optimal level under the applied electric field with the formation of OCOO, the reaction barrier of 0.55 eV is still higher than the barrier of 0.35 eV on Ag_{ML}/Nb_2C. To sum up, Ag_{ML}/Nb_2C has the higher efficiency for CO oxidation. Here, we screened Ag_{ML}/Nb_2C out from a series of M_{ML}/Nb_2C and verified that it had high CO oxidation efficiency, which would

Table 5. The Rate-determining steps and corresponding reaction barriers (in eV) of CO oxidation reaction in different systems.

Systems	Rate-determining step	$E_{barrier}$(eV)
Pd(1 0 0) [33]	$CO + O \rightarrow CO_2$	0.78
Pd(1 1 1) [33]	$CO + O \rightarrow CO_2$	0.91
Ag(1 1 1) [29]	$CO + O_2 \rightarrow CO_2 + O$	1.03
Ag_{ML}/WC(0 0 0 1) [34]	$CO + O \rightarrow CO_2$	0.48
Mn-doped graphene [35]	$CO + O_2 \rightarrow OCOO$	0.55

provide a theoretical basis for the design of electrode materials for PEMFCs.

4. Conclusion

Based on the first-principles calculation, the stability of M_{ML}/Nb_2C was systematically studied. It was found that low coverage of all the metal atoms studied tended to form a single layer on Nb_2C rather than metal bulk or clusters. The adsorption of small gas molecules on the different M_{ML}/Nb_2C systems was analyzed. By comparing the adsorption properties of small gas molecules, we proposed Ag_{ML}/Nb_2C as the promising candidate catalyst for CO oxidation. Through the exploration of different reaction mechanisms of CO oxidation on Ag_{ML}/Nb_2C, we found that the LH mechanism had the minimum energy barrier of 0.35 eV, and the rate-limiting step was the oxidation of CO by the adsorbed oxygen atom. The suitable adsorption strength and low CO oxidation barrier made the Ag_{ML}/Nb_2C an efficient catalyst with high CO-tolerance and high CO conversion efficiency, which would provide a theoretical basis for designing of PEMFCs electrode materials.

Acknowledgments

The financial supports from the National Natural Science Foundation of China (Grant Nos. 11874141, U1804130, 11904084 and 11474086) and the Henan Overseas Expertise Introduction Center for Discipline Innovation (CXJD2019005), and the computational resources provided by the High Performance Computing Center of Henan Normal University are acknowledge.

ORCID iDs

Xilin Zhang https://orcid.org/0000-0002-7141-5700
Zongxian Yang https://orcid.org/0000-0002-3015-3804

References

[1] Naguib M, Mochalin V N, Barsoum M W and Gogotsi Y 2014 *Adv. Mater.* **26** 992–1005
[2] Anasori B, Xie Y, Beidaghi M, Lu J, Hosler B C, Hultman L, Kent P R, Gogotsi Y and Barsoum M W 2015 *ACS Nano* **9** 9507–16
[3] Lei J C, Zhang X and Zhou Z 2015 *Frontiers Phys.* **10** 276–86
[4] Kumar H, Frey N C, Dong L, Anasori B, Gogotsi Y and Shenoy V B 2017 *ACS Nano* **11** 7648–55
[5] Khazaei M, Ranjbar A, Arai M, Sasaki T and Yunoki S 2017 *J. Mater. Chem.* C **5** 2488–503
[6] Xu Z, Lei J, Wu D, Zhao X, Yu J and Zhen Z 2016 *J. Mater. Chem.* A **4** 4871–6
[7] Cheng C, Zhang X, Yang Z and Zhou Z 2018 *ACS Appl. Mater. Interfaces* **10** 12318
[8] Guo Z, Zhou J, Zhu L and Sun Z 2016 *J. Mater. Chem.* A **4** 11446–52
[9] Michael N, Joseph H, Jun L, Cook K M, Lars H, Yury G and Barsoum M W 2013 *JACS* **135** 15966–9
[10] Handoko A D, Khoo K H, Tan T L, Jin H and Seh Z W 2018 *J. Mater Chem.* A **6** 21885–90
[11] Gao G, O'Mullane A P and Du A 2017 *ACS Catal.* **7** 02754
[12] Pandey M and Thygesen K S 2017 *J. Phys. Chem.* C **121** 05270
[13] Haruta M, Tsubota S, Kobayashi T, Kageyama H, Genet M J and Delmon B 1993 *J. Catal.* **144** 175–92
[14] Kung H H, Kung M and Costello C 2003 *J. Catal.* **216** 425–32
[15] Liu J H, Wang A Q, Chi Y S, Lin H P and Mou C Y 2005 *The J. Phys. Chem.* B **109** 40–3
[16] Schubert M M, Hackenberg S, Van Veen A C, Muhler M, Plzak V and Behm R J 2001 *J. Catal.* **197** 113–22
[17] Kan D, Zhang X, Zhang Y and Yang Z 2018 *J. Power Sources* **378** 691–8
[18] Lin S, Ye X, Johnson R S and Guo H 2013 *J. Phys. Chem.* C **117** 17319–26
[19] Ahmed B, Anjum D H, Gogotsi Y and Alshareef H N 2017 *Nano Energy* **34** 249–56
[20] Dall'Agnese Y, Rozier P, Taberna P L, Gogotsi Y and Simon P 2016 *J. Power Sources* **306** 510–5
[21] Chen C *et al* 2018 *Angew. Chem., Int. Ed.* **57** 1846–50
[22] Delley B 2002 *Phys. Rev.* B **66** 155125
[23] Halgren T A and Lipscomb W N 1977 *Chem. Phys. Lett.* **49** 225–32
[24] Alexandre T and Matthias S 2009 *Phys. Rev. Lett.* **102** 073005
[25] Monkhorst H J and Pack J D 1976 *Phys. Rev.* B **13** 5188
[26] Perdew J P, Burke K and Ernzerhof M 1996 *Phys Rev Lett.* **77** 3865
[27] Khazaei M, Arai M, Sasaki T, Chung C Y, Venkataramanan N S, Estili M, Sakka Y and Kawazoe Y 2013 *Adv. Funct. Mater.* **23** 2185–92
[28] Lei X, Mbamalu G and GandQin C 2017 *J. Phys. Chem.* C **121** 2635–42
[29] Su H Y, Yang M M, Bao X H and Li W X 2008 *J. Phys. Chem.* C **112** 17303–10
[30] An W, Pei Y and Zeng X 2008 *Nano Lett.* **8** 195–202
[31] Molina L and Hammer B 2005 *J. Catal.* **233** 399–404
[32] Mao K, Li L, Zhang W, Pei Y, Zeng X C, Wu X and Yang J 2014 *Sci. Rep.* **4** 5441
[33] Zhang C and Hu P 2001 *JACS* **123** 1166–72
[34] Zhao Y, Zhang X and Yang Z 2019 *Phys. Lett.* A **383** 2436–42
[35] Xu X Y, Guo H and Zhao C 2017 *J. Phys. Chem.* C **121** 27983–91